1

Large-scale Controls on Atlantic Tropical Cyclone Activity

on Seasonal Time Scales

4

5

6

Young-Kwon Lim[1,2], Siegfried D. Schubert[1],

Oreste Reale[1,3], Andrea M. Molod[1,4], Max J. Suarez[1,3] Benjamin M. Auer[1,5]

9

Corresponding author: Young-Kwon Lim (Young-Kwon.Lim@nasa.gov)

11

[1]Bldg. 33, code 610.1, 8800 Greenbelt Rd.,

Global Modeling and Assimilation Office, NASA/GSFC, Greenbelt, Maryland, 20771

[2]Goddard Earth Sciences Technology and Research, I. M. Systems Group

[3]Goddard Earth Sciences Technology and Research, Universities Space Research

Association (USRA)

[4]Earth System Science Interdisciplinary Center,

University of Maryland, College Park, Maryland

[5]Science Systems and Applications Inc. (SSAI)

20

21

22

23

Abstract

Interannual variations in seasonal tropical cyclone (TC) activity (e.g., genesis frequency and location, track pattern, and landfall) over the Atlantic are explored by employing observationally-constrained simulations with the NASA Goddard Earth Observing System version (GEOS-5) atmospheric general circulation model. The climate modes investigated are El Niño-Southern Oscillation (ENSO), the North Atlantic Oscillation (NAO), and the Atlantic Meridional Mode (AMM).

The results show that the NAO and AMM can strongly modify and even oppose the well-known ENSO impacts, like in 2005, when a strong positive AMM (associated with warm SSTs and a negative SLP anomaly over the western tropical Atlantic), led to a very active TC season with enhanced TC genesis over the Caribbean Sea and a number of landfalls over North America, under a neutral ENSO condition. On the other end, the weak TC activity during 2013 (characterized by weak negative Niño index) appears caused by a NAO-induced positive SLP anomaly with enhanced vertical wind shear over the tropical North Atlantic. During 2010, the combined impact of the three modes produced positive SST anomalies across the entire low-latitudinal Atlantic and a weaker subtropical high, leading to more early recurvers and thus fewer landfalls despite enhanced TC genesis. The study provides evidence that TC number and track are very sensitive to the relative phases and intensities of these three modes, and not just to ENSO alone. Examination of seasonal predictability reveals that predictive skill of the three modes is limited over tropics to sub-tropics, with the AMM having the highest predictability over the North Atlantic, followed by ENSO and NAO.

1. Introduction

Seasonal tropical cyclone (TC) activity (e.g., genesis frequency and location, track patterns, landfall, life cycle, etc.) over the North Atlantic is characterized by considerable year-to-year variability. A number of atmospheric general circulation models (AGCMs) and statistical models have demonstrated some ability to reproduce interannual variations in TC (hurricane, tropical storm, and tropical depression) frequency over the past few decades (Klotzbach and Gray 2004; LaRow et al. 2008; Zhao et al. 2009; Kim and Webster 2010; Putman and Suarez 2011; Chen and Lin 2013; Bacmeister et al. 2014; Vecchi et al. 2014; Murakami et al. 2015; Wang et al. 2015). The latest NASA "Nature Run", produced by the Global Modeling and Assimilation Office (GMAO) and documented in Gelaro et al. (2015), is particularly remarkable for its high resolution (~7km). It has produced differences in TC activity between 2005 and 2006, which were consistent with observations over each ocean basin including some "difficult" basin such as the northern Indian Ocean, where generally global models perform less than optimally partly due to shorter lifespan and more erratic TC tracks, compared to the Atlantic and Pacific (e.g., Reale et al. 2009).

However, operational forecasting agencies do not issue sub-seasonal and seasonal predictions of the societally most important aspects such as track and landfall distribution (http://www.cpc.noaa.gov/products/outlooks/hurricane-archive.shtml). An active TC season in which most storms are "early recurvers" (i.e., Cape Verde TCs that recurve northeastward at about 45°W instead of crossing the Atlantic) may have less societal impact than an inactive season with a single strike over a highly populated area (e.g, Blake and Gibney 2011). The 2010 TC season is one of those cases in point. The primary factors (e.g., sea surface temperature (SST) and El Niño Southern Oscillation (ENSO)) assumed to control TC activity suggested an active

71 TC genesis (http://www.cpc.noaa.gov/products/outlooks/hurricane2010/May/hurricane.shtml).

72 However, no hurricanes made landfall over the United States (US) (Bell et al. 2011; Wang et al.

73 2011)- in spite of the large number of observed TCs.

74   It has been accepted for more than 50 years that the sign of SLP anomalies over the tropical

75 Atlantic (TA, defined as in Knaff 1997) is correlated with TC activity (Knaff 1997). However,

76 increasing complexity has been added by several recent studies indicating that TC occurrence is

77 related to climate variability through changes in both circulation and thermodynamic conditions

78 (Kossin and Camargo 2009; Kossin et al. 2010; Patricola et al. 2014) controlled by a synergy

79 between the Atlantic Meridional Mode (AMM) (Chiang and Vimont 2004) and ENSO, which are

80 also found to modulate deep convection throughout the tropics (e.g., Colbert and Soden 2012).

81 Moreover, the Madden Julian Oscillation (MJO) appears to control TCs throughout the tropical

82 Atlantic (Mo 2000; Maloney and Hartmann 2000; Camargo et al. 2009; Klotzbach 2010;

83 Klotzbach and Oliver 2015). In addition, a number of studies (Elsner 2003, Kossin et al. 2010)

84 suggested that the North Atlantic Oscillation (NAO) (Wallace and Gutzler 1981; Barnston and

85 Livezey 1987) affects TCs, with the negative NAO eroding the western flank of the North

86 Atlantic subtropical high and allowing TCs to become recurvers. In apparent contrast, Xie et al.

87 (2005) found that TC landfall number along the US east coast is negatively correlated with the

88 NAO phase. The ENSO phase also seems to affect the probability of landfalling TCs (e.g.,

89 O'Brien et al. 1996; Bove et al. 1998; Larson et al. 2005) as well as the presence of TCs in the

90 Caribbean (Tartaglione et al. 2003). Smith et al. (2007) suggest that ENSO impacts on

91 landfalling frequencies over the US is largest on the East Coast from Georgia to Maine, and less

92 so over Florida and the Gulf Coast.

93   In terms of mechanisms, ENSO and AMM are known to impact shear (e.g., Kossin and

4

94 Vimont 2007) with La Niña (El Niño) and positive (negative) AMM driving low (high) shear

95 anomalies (Aiyyer and Thorncroft 2006; Shaman et al. 2009). Smirnov and Vimont (2011)

96 showed that a reduction (enhancement) in vertical wind shear occurs with the positive (negative)

97 SST anomalies over the subtropical North Atlantic during the positive (negative) AMM.

98 Camargo et al. (2007) confirmed that the dynamical role of wind shear is as important as any

99 thermodynamic impacts in El Niño years. Patricola et al. (2014) also found that mid-tropospheric

100 moisture as a thermodynamic impact plays an equally important role compared to vertical wind

101 shear in controlling Atlantic TC activity during the AMM.

102   Despite the vast number of studies focused on the understanding of the physical processes

103 impacting TC activity, surprisingly poor seasonal predictions (in terms of TC counts) are

104 sometimes released. For example, strong TC activity with 14-20 TCs was forecasted for year

105 2013 due to above-average SSTs across the tropical Atlantic and no El Niño conditions ahead of

106 TC   season   (http://www.cpc.noaa.gov/products/outlooks/hurricane2013/May/hurricane.shtml).

107 However, the 2013 TC season was characterized by a strong positive sea level pressure (SLP)

108 anomaly and wind shear, conducive to weak TC activity (Blake 2014) with 14 TCs, most of

109 which   were   short-lived.   The   2006   TC   season   was   predicted   to   be   active

110 (http://www.noaanews.noaa.gov/stories2006/s2634.htm, 13-16 TCs forecasted), which did not

111 turned out to be the case (10 TCs with few landfalls). Some authors have suggested a more

112 important role for dust than dynamical modes (e.g., Lau and Kim 2007). On the other hand, the

113 very active TC season in 2005 (observation: 29 (Fig. 2a), operational forecast: 12-15 TCs

114 (http://www.cpc.noaa.gov/products/outlooks/hurricane2005/May/hurricane.html))   and   2010

115 (http://www.cpc.noaa.gov/products/outlooks/hurricane2010/May/hurricane.html, observation: 21

116 (Fig. 4a), forecast: 14-23) was reasonably forecasted. However, those two TC seasons were

117   characterized by very different distributions of TC genesis locations and landfalls, which are not

118   products provided by the current operational forecasting agencies on seasonal time scales.

119   While the possibility exists that many more causes, some unknown, affect TC activity, the

120   main objective of this study is to improve our understanding of how the dynamics of large-scale

121   climate variability associated with 3 well-studied modes (ENSO, the AMM, and the NAO) can

122   impact North Atlantic seasonal TC activity. Moreover, this work aims at assessing the ability to

123   predict these major modes of variability using a state-of-the-art atmospheric general circulation

124   model (AGCM). An observational analysis combined with partially constrained simulations with

125   the National Aeronautics and Space Administration (NASA) Goddard Earth Observing System

126   Model version 5 (GEOS-5) AGCM (Rienecker et al. 2008) is carried out. Specifically, we use a

127   "replay" (see section 2) capability that takes advantage of the Modern-Era Retrospective

128   Analysis for Research and Applications (MERRA) reanalysis (Rienecker et al. 2011) to constrain

129   large-scale aspects of the atmosphere in the GEOS-5 simulations.

130   The paper is organized as follows. The analysis data, GEOS-5 model, and the experimental

131   design are described in Section 2. Section 3.1 presents and compares the TC track statistics

132   produced in each of the model experiments. We then quantify the impact of the dominant climate

133   modes of variability on the Atlantic TC activity for selected recent years and discuss the

134   atmospheric large-scale constraints necessary to control the seasonal TC activity (sections 3.2-

135   3.5). Additionally, we explore if this large-scale constraint can also reproduce the observed

136   relationship between TC genesis frequency and the phase of the Madden-Julian Oscillation (MJO)

137   (section 3.6). In section 3.7, we assess the predictability of the dominant climate modes for the

138   last 9 hurricane seasons (2005-2013) simulated by the GEOS-5 AGCM. A discussion and

139   conclusions are given in Section 4.

140

2. Data, model and experimental design

2.1 Data and model

The study employs: a) the MERRA data (Rienecker et al. 2011) used at native horizontal resolution of 0.5° latitude×0.6667° longitude; and b) model simulations, making use of the NASA GEOS-5 AGCM (Rienecker et al. 2008; Molod et al. 2012). The investigation is focused over North America and the Atlantic Ocean, covering the Atlantic TC seasons (June through November) from 2005 through 2013. Key variables include SST, SLP, lower (850hPa) and upper (200hPa) level horizontal wind, relative humidity at 700hPa, and upper-level (250hPa) geopotential height. The observed TC best track data (HURDAT2) (see Figs. 2a-5a) are obtained from the National Hurricane Center (Landsea and Franklin, 2013). This hurricane database is a post-storm reanalysis which includes all available observations, including from systems which are not available in real time, and is documented online at: http://www.aoml.noaa.gov/hrd/hurdat/newhurdat-format.pdf.

The NASA GEOS-5 was run with 72 hybrid-sigma vertical layers, extending to 0.01 hPa, and ~0.5° latitude/longitude horizontal resolution. The model uses the finite-volume dynamics of Lin (2004), along with a modified version of the Relaxed Arakawa Schubert (RAS) convection scheme of Moorthi and Suarez (1992). A stochastic Tokioka constraint (Tokioka et al. 1988; Lim et al. 2015) is applied to the convective plumes, leading to improved TC genesis without negatively impacting the mean climate (Reed and Jablonowski 2011; Zhao et al. 2012; Lim et al. 2015). The model employs a prognostic cloud microphysics scheme (Bacmeister et al. 2006) and the catchment land surface model developed by Koster et al. (2000). Further details about the GEOS-5 AGCM can be found in Rienecker et al. (2008) and Molod et al. (2012).

7

163

2.2 Model Experiments

One of this study's goals is to quantify the dominant large-scale controls on North Atlantic

TC tracks, by reproducing the observed TC track statistics in the GEOS-5 simulations and

adopting a replay methodology (Rienecker et al. 2008) to systematically constrain different

aspects of the simulations.

The Incremental Analysis Update (IAU) approach developed by Bloom et al. (1996), and

implemented in the GEOS-5 Data Assimilation System (DAS) is an essential element of our

procedure. The IAU approach allows to insert gradually analysis increments produced during the

assimilation cycle in the model and has been generalized so that the model can be "replayed"

against an existing analysis (MERRA in this study). The IAU (Fig. 1) reads in an existing

analysis field at the analysis time, computes an analysis increment (the difference from the first

guess) generally over a 6 hour interval, rewinds 3 hours, and forces the model with a scaled

version of the increment over the next 6 hours. The model is then run another 3 hours without the

analysis increment forcing to provide the next first guess field, at which point the cycle repeats.

The replay process therefore consists of a continuous model run that is forced by analysis

increments changing every 6 hours. Since the experiments' goal is the evaluation of the large-

scale atmospheric control of TC tracks, the analysis increments are spatially filtered (spectral

triangular truncation) to retain only the largest planetary scales. It should be emphasized that this

filtering procedure does not directly affect or constrain the TCs. The years selected (2005, 2006,

2010 and 2013) are characterized by very different TC intensities and tracks, thus providing a

wide range of variability within a limited sample. Three different sets of experiments are

performed for the large-scale constraints, with analysis increments: i) filtered to retain only the

186 first five total wavenumbers (hereafter R5W); ii) filtered to retain the first eight total

187 wavenumbers (R8W), and iii) unconstrained (unfiltered), as a free running simulation here

188 referred to as "Nature Run" (NR). All simulations are done with prescribed weekly sea surface

189 temperature (SST) forcing (the HadISST of Rayner et al. 2003). Each set of experiments

190 consists of three ensemble members initialized from MERRA atmospheric data on May 1st , 2nd,

191 and 3rd of each year.

192

193 3. Results

194 3.1 TC tracks

195 The TC tracks for June through November of each year (computed with the same TC

196 detection and tracking algorithm used by Vitart et al. 2003, Knutson et al. 2007, and LaRow et al.

197 2008) are shown in Figs. 2-5. TC threshold values for relative vorticity, maximum wind speed,

198 warm core, SLP deepening and minimum duration time (Table 1) are similar to those suggested

199 by Walsh et al. (2007) for a 0.5° horizontal resolution model. A key result is that all three

200 experiments successfully reproduce the interannual variations of TC numbers. For example, the

201 experiments indicate an active season (19-22) in 2005 (Fig. 2), although fewer than the observed

202 29, and produce from 18 to 21 TCs for the active season of 2010, which is close to the observed

203 20 TCs (Fig. 4). Similarly, the inactive seasons of 2006 and 2013 are well captured by the

204 experiments (Figs. 3 and 5).

205 A prominent difference between the active 2005 and 2010 seasons is the relative scarcity of

206 Cape Verde systems (i.e., systems whose genesis occur over the Eastern Atlantic, close to Africa)

207 in 2005 with respect to 2010 (Fig. 4a). The fewer instances of eastern Atlantic TC genesis in

208 2005 season appear closely linked to the negative SLP anomalies in the central and western

209 Atlantic (Fig. 2a). The 2005 season was not only characterized by exceptional TC genesis, but

210 also by a number of landfalls over the North American continent (Fig. 2a, Table 2). The spatial

211 pattern of TC tracks in the three experiments suggests sensitivity to the simulated SLP anomaly

212 distribution. In fact, the R8W run produces a TC pattern closest to the observed in terms of

213 landfall (Fig. 2c, 3–4th rows in Table 2) and also the largest negative SLP anomalies centered

214 over the Gulf of Mexico and Caribbean Sea (Figs. 2a,c). In contrast, the NR shows an

215 excessively extended SLP anomaly with more Cape Verde systems (Figs. 2d,g,j) and fewer

216 landfalls over the US compared with the other runs (Fig. 2d, Table 2). The R5W shows an

217 intermediate situation between the two in terms of landfalls over the US (3rd row in Table 2).

218   The inactive 2006 TC season is also best represented by the R8W (Fig. 3). The observations

219 (Fig. 3a) show only 10 TCs and two landfalls (Table 2) with the remaining TCs being recurvers

220 or tracking well to the east of the US coast. Again, the good representation of TC tracks in R8W

221 finds good correspondence with realistic SLP anomalies (Figs. 3a,c). In contrast, the NR run

222 produces more landfalls (Figs. 3d,g, 5–6th rows in Table 2) than the other two experiments and

223 the observations, while the R5W (Fig. 3b) shows fewer recurvers than observed, and more

224 landfalls than the R8W but fewer than the NR over the US (5th row in Table 2). As noted before,

225 the ability of producing a realistic SLP anomaly seems to be connected with a realistic track

226 distribution.

227   In spite of 2010 being another active TC season, the TC track pattern differs significantly

228 from 2005. The observations in Fig. 4a clearly show that TC genesis locations are zonally

229 distributed across the subtropical North Atlantic, in good correspondence with zonally elongated

230 negative SLP anomalies. Wang et al. (2011) argued that the negative SLP anomalies in 2010

231 could be resulting from a strong eastward expansion of the Atlantic warm pool and may inhibit

232   the westward expansion of the positive SLP anomaly in the eastern Atlantic. This pattern could

233   be a prominent cause for TCs to recurve far away from the US continent, producing fewer

234   landfalls despite active TC genesis often attributed to La Niña conditions. Landfalling TCs are

235   associated either with westward moving TCs crossing the Atlantic toward Central America or

236   with systems generated in the Caribbean. TC tracks generated by the R8W and R5W runs are

237   more realistic than the NR run (Figs. 4b-d), including the number of US landfalls, which are

238   strongly overestimated in the NR (cf. Figs. 4d,g, 7th row in Table 2).

239   2013 was an inactive TC season, with positive SLP anomalies throughout the North Atlantic

240   (Fig. 5a). All three experiments could reproduce the SLP pattern over the Atlantic (Figs. 5b-d),

241   but the NR generated a larger number of TCs with several tracks through the Caribbean Sea and

242   the Gulf of Mexico, overestimating the landfalls over the southeastern US, (Figs. 5d,g, 9th row in

243   Table 2). On the other hand, R8W and R5W produce a smaller number of landfalls and, most

244   important, a prominent feature of the 2013 season: several Cape Verde systems crossing the

245   Atlantic westward with an almost straight trajectory. This finding seems to agree with Elsner

246   (2003), who suggested that a positive anomaly in the North Atlantic subtropical high associated

247   with the NAO favors relatively straight westward TC tracks with little recurvature. The possible

248   impact of the positive NAO on the TC activity for this year will be examined in the next section.

249

250   3.2 Three leading climate modes that impact Atlantic TC activity

251   A rotated EOF (REOF) technique (Richman 1986) is first employed to investigate the

252   variability of seasonal TC track and landfall patterns in the experiments, with the goal of

253   capturing the leading climate modes that could explain the role of monthly SST in modulating

254   Atlantic TC activity. The three leading SST climate modes are ENSO, the North Atlantic

255 Oscillation (NAO) (Wallace and Gutzler 1981; Barnston and Livezey 1987) and the Atlantic

256 Meridional Mode (AMM) (Vimont and Kossin 2007; Smirnov and Vimont 2011). These

257 findings are in good agreement with Kossin et al. (2010).

258   The eigenvectors (the spatial distributions) together with the corresponding principal

259 component (PC) time series of the three modes are shown in Figure 6. All eigenvectors and PC

260 time series are plotted for the positive phase, together with the traditional index time series of

261 these modes (data from the NOAA Climate Prediction Center (CPC) available at:

262 ftp://ftp.cpc.ncep.noaa.gov/wd52dg/data/indices/tele_index.nh). The PC time series are in good

263 agreement with the phases of the ENSO and AMM indices (Figs. 6d,f), whereas the PCs,

264 correspond with the NAO in 2005, 2006, 2007, 2010, 2012 and 2013, but not in 2008, 2009 and

265 2011 (Fig. 6e). It is possible that since the NAO is primarily an atmospheric mode (Barnston and

266 Livezey 1987) it is marginally affected by SST.

267   The El Niño mode is characterized by positive SST anomalies over the tropical eastern

268 Pacific, positive anomalies over the extratropical Atlantic, and negative anomalies across the

269 tropical Atlantic and the Caribbean (Fig. 6a) (Deser et al. 2010), which contribute to unfavorable

270 conditions for TC genesis, with the opposite pattern during the cold ENSO phase.

271   The NAO-related SST REOF shown in Fig. 6b is characterized by a north-south tripole

272 across the extra-tropical Atlantic. Two zones of negative SST anomalies occur between 20°-

273 30°N and 50°-60°N, separated by a zone of positive anomalies. The tropical Atlantic is

274 characterized by relatively weak negative (positive) SST anomalies during the positive (negative)

275 phase of the NAO, providing unfavorable (favorable) conditions for TC activity. This result

276 appears in agreement with Elsner and Jagger's (2006) statistical assessment of the NAO phase

277 impact on TCs.

278   It is particularly noteworthy that the positive phase of the AMM mode (Fig. 6c)

279   characterized by positive SST anomalies throughout the tropical Atlantic as far as ~30°N

280   (Chiang and Vimont 2004), can be sufficiently strong to offset the negative SST anomalies over

281   the same region associated with El Niño events (cf. Fig. 6c and 6a). Figure 6f shows that both

282   2005 and 2010 are characterized by strong positive AMM episodes, while 2006 and 2013 are

283   characterized by near-neutral (or weak positive) AMM conditions.

284

285   3.3 Regressed atmospheric anomalies associated with the large-scale leading modes

286   The next step is to regress the leading modes identified above (ENSO, NAO and AMM)

287   against each PC time series of ENSO, NAO, and AMM for the years 2005-2013, to assess their

288   impact on atmospheric variables such as SLP, z250, vertical wind shear and relative humidity at

289   700hPa (RH700). For example, the regressed atmospheric anomalies for the ENSO mode at grid

290   point (*x*,*y*) is given as

291         $$R_{ENSO}(x,y) = \sum_{t=1}^{nt} T(x,y,t) \cdot TS_{ENSO}(t), \tag{1}$$

292   where $T(x,y,t)$ is the anomaly field in question at time step *t*, and $TS_{ENSO}(t)$ represents the

293   normalized monthly PC time series for ENSO. *nt* is the length of the analysis period. Here *nt* is

294   given as 108 (9 years × 4 months (June-September) × 3 members). Similar calculations are made

295   for the NAO and AMM.

296   Figure 7 shows the atmospheric fields regressed against ENSO. The observed response to

297   El Niño shows the expected pattern of negative SLP anomalies over the eastern tropical Pacific,

298   and positive SLP anomalies at tropical to subtropical Atlantic, suggestive of unfavorable

299   conditions for TC genesis over the regions (Fig. 7a). This pattern is reproduced in both the R8W

300   and R5W runs (Figs. 7e,i) but not realistically in the NR run (Fig. 7m). The RH700 exhibits

301   negative anomalies associated with El Niño, primarily over the Caribbean Sea and the tropical

13

302 western-central Atlantic (Figs. 7b,f,j,n), where the positive SLP anomalies dominate. As for the

303 vertical wind shear, only the R8W run produces realistic vertical wind shear anomalies (Figs.

304 7c,g,k,o). The climatological vertical wind shear over the Atlantic during the TC season is

305 generally controlled by the tropical easterly jet (TEJ) and by subtropical high-level winds. While

306 the TEJ is confined at latitudes lower than 15°N and is the prominent cause of easterly shear

307 (hatched in Figs. 7c,g,k,o), westerly shear is controlled by either easterly flow decreasing with

308 height, or by upper-level westerly flow which may be associated with the subtropical jet. Thus,

309 the positive wind shear anomaly across the US and the Atlantic at ~30–40°N represents

310 enhanced vertical westerly shear, and appears dynamically linked to an enhanced upper-level

311 westerly subtropical jet during El Niño (Zhu et al. 2012), which opposes the northward

312 progression of TCs.

313 Figure 8 is the same as Fig.7, but for the NAO mode. The top panel in Fig. 8 shows that the

314 North Atlantic midlatitudes are dominated by positive SLP anomalies during the positive NAO,

315 creating unfavorable conditions for TC genesis and evolution, in agreement with Knaff (1997)

316 and Kossin et al. (2010) who also found that positive (negative) SLP anomalies associated with

317 the positive (negative) phase of the May-June NAO are correlated with a local decrease (increase)

318 in TC genesis. In addition, Xie et al. (2005) argued that the negative NAO favors more

319 landfalling hurricanes over the US southeast region. Our model results indicate that the R8W is

320 again more realistic in reproducing the details (especially the gradients) of the observationally-

321 based regressed SLP pattern (Figs. 8a,e,i,m) with respect to the R5W and the NR.

322 The observations and R8W suggest that the positive phase of the NAO is associated with

323 positive RH700 anomalies over the western subtropical Atlantic, to the southwest of the positive

324 SLP anomaly in mid-latitudes Atlantic (Figs. 8b,f) and with an area of negative RH700

325   anomalies over the central to eastern extra-tropical Atlantic, in correspondence with the core of

326   the positive SLP anomalies. The positive NAO is also associated with enhanced vertical westerly

327   shear along ~20°N (Figs. 8c,g,k,o). The negative upper-level height anomaly (Figs. 8d,h) at

328   ~30°N and associated upper-level westerly anomaly to the south of it is likely to drive this strong

329   vertical westerly shear along ~20°N, contributing to very unfavorable conditions for TC genesis

330   over the subtropical North Atlantic. Here again, the R8W run is the most realistic (with respect to

331   R5W and NR) against the observed anomalies.

332   Figure 9 highlights the prominent role exerted by the AMM positive (negative) phase on

333   favorable (unfavorable) conditions for TC genesis. In particular, negative SLP anomalies and

334   drastic weakening of vertical westerly shear, which correspond to the positive phase, are

335   conditions favorable to TC genesis over the western and central Atlantic (Figs. 9a,c,e,g,i,k,m,o)

336   in agreement with Vimont and Kossin (2007), Kossin et al. (2010), Smirnov and Vimont (2011)

337   and Patricola et al. (2014). Large positive RH700 anomalies over the subtropical Atlantic region

338   (Figs. 9b,f,j,n) are associated with the AMM and are well reproduced in all experiments.

339   However, a comprehensive verification of the experiments shows that, in general, the regressed

340   AMM patterns resemble reasonably well the observations, with the R8W being by far the best

341   (Fig. 9). Overall, Figs. 7-9 indicate that the R8W run provides the most realistic constraints on

342   TC activity linked to the three large-scale climate modes, while also better reproducing the

343   observed characteristics of the TC tracks (Figs. 2-5).

344

345   3.4 Reconstructing the interannual variations of atmospheric anomalies

346   The combined potential impacts of ENSO, the NAO and the AMM on Atlantic TC activity

347   during each year is explored by creating a linear combination of the regressed anomalies and

348 corresponding PC time series. For example, the reconstructed $T_{ENSO}(x, y, t)$ for the ENSO mode

349 at grid point (x,y) and time t is defined as

350 $$T_{ENSO}(x, y, t) = R_{ENSO}(x, y) \cdot TS_{ENSO}(t), \qquad (2)$$

351 where $R_{ENSO}(x, y)$ is the regressed atmospheric field for the ENSO mode (1) and

352 $TS_{ENSO}(t)$ is the normalized monthly PC time series for the ENSO mode. This procedure helps

353 identify the effectiveness of these modes in reconstructing the observed atmospheric anomalies.

354   Figure 10 compares the observed SLP anomalies in 2005, 2006, 2010 and 2013 with the

355 ones obtained in the experiments R8W and NR by combining the effects of ENSO, NAO and

356 AMM modes. This comparison allows us to discern the model-produced atmospheric anomalies

357 with and without the large-scale constraints (i.e., R8W versus NR). The R8W run (Figs. 10e-h) is

358 particularly effective in reproducing the observed SLP anomalies (Figs. 10a-d) when the

359 contributions of the three climate modes are acting together. In particular, the strong negative

360 SLP anomaly over the central to western Atlantic which is indicative of enhanced TC genesis in

361 2005 (see Figs. 2a,c) is realistically reproduced (Figs. 10a,e). In the eastern Atlantic, the

362 observed positive SLP anomaly is slightly hinted at in the R8W but totally missed in the NR (Fig.

363 10i), which leads to overestimated TC genesis in the NR over the region. In addition, the vast

364 negative SLP anomaly joining the western tropical Atlantic with the mid latitude northeastern

365 Atlantic is consistent with the typical path of early recurvers (non-landfalling TCs) which occur

366 in the NR more than in the observations and R8W run (Figs. 2c,d).

367   Positive SLP anomalies characterize both the R8W and NR in 2006, consistent with reduced

368 TC genesis, although the SLP zonal gradients in the central Atlantic are better characterized in

369 the R8W.

370   In complete contrast with 2006, in 2010 the North Atlantic was characterized by a negative

371 SLP anomaly over most of the domain, with a positive SLP anomaly in the eastern mid-latitudes

372 (see section 3.1, and Figs. 4a,c). The SLP anomaly pattern is again successfully captured by the

373 R8W run (compare Figs. 10c,g,k). While the synergy of weak El Niño and near-neutral AMM in

374 2006 contribute to the positive SLP anomaly (see the impact of El Niño and the positive AMM

375 on the SLP shown in Figs. 7a and 9a) over the western Atlantic and negative anomaly over the

376 eastern Atlantic, the pattern in 2010 is reversed with a synergy between La Niña and a positive

377 AMM phase, which lead to enhanced activity over the western Atlantic.

378   In spite of the Niño index being negative in both 2010 and 2013, the SLP distribution

379 between the two is very different. While the negative Niño index caused positive SLP anomalies

380 over the tropical eastern Pacific in both years (larger in 2010 than in 2013), the Atlantic region

381 was dominated by a negative SLP anomaly in 2010 and by a positive SLP anomaly in 2013

382 (compare Figs. 10c and 10d). The positive SLP anomaly over the Atlantic in 2013 can be

383 explained by the presence of a positive NAO, strong enough to counteract the effects of the

384 neutral ENSO with weak negative Niño indices, as will be discussed later in the context of Table

385 3. As in the other cases, the R8W reproduces the anomalies over the subtropical North Atlantic

386 (Figs. 10d,h), better than the NR.

387   We next extend our investigation to include the vertical wind shear and relative humidity

388 fields (Fig. 11). While shear is often assumed to be westerly, easterly shear is also important,

389 particularly at the early phases of TC genesis. Strong westerly shear can dissipate a mature

390 hurricane, but easterly shear, even when moderate, can inhibit or delay the transformation of an

391 open easterly wave into a closed circulation. Figures 11a,e,i suggest that the combined impacts

392 of ENSO, the AMM, and the NAO lead to wetter conditions and weakening of vertical westerly

393 shear over the Caribbean and western Atlantic during 2005, consistent with enhanced TC genesis

17

394   over the region and reduced number of Cape Verde systems over the eastern Atlantic (Fig. 2a

395   and Fig. 10a). During 2006, a positive vertical westerly shear anomaly is found between 10°-

396   20°N, along with a weak negative humidity anomaly over the western-central tropical Atlantic,

397   in both the observations and the R8W run (Figs. 11b,f). The NR run, in contrast, produces a

398   positive humidity anomaly over the Gulf of Mexico and subtropical Atlantic (Fig. 11j). In 2010,

399   the overall weakeness of vertical westerly shear over the subtropical North Atlantic suggest

400   strong TC activity including Cape Verde systems. These patterns are captured well in the R8W

401   and, to a lesser extent, in the NR (Figs. 11c,g,k).

402   Finally, the very inactive 2013 season, in spite of being a weak negative Niño index year, is

403   perhaps the most interesting case to demonstrate the importance of the combined action of the

404   three modes. Figure 11d indicates that 2013 was characterized by moderate to strong vertical

405   westerly shear throughout the entire tropical Atlantic, with dry conditions as well over the central

406   Atlantic. These patterns, according to Fogarty and Klotzbach (2014), may have contributed to the

407   poor skill of most operational seasonal TC forecasts. The R8W run was able to reproduce the

408   strong westerly wind shear and dry condition over the subtropical Atlantic (~20°N) (Figs. 11d,h)

409   except the very dry area over the central Atlantic between 10-15°N (Fig. 11d), suggesting other

410   contributing forcings. The NR could not reproduce the observed shear and humidity distributions

411   successfully, resulting in unrealistic TC track patterns (Fig. 5).

412

413   3.5 Relative contribution of the leading modes to seasonal anomalies

414   Figures 10 and 11 suggest that the interannually changing characteristics of the seasonal

415   atmospheric anomalies can be at least partially controlled by the interaction of the three leading

416   modes of variability. In order to examine the relative contributions of each mode, SLP, z250,

417   wind shear, and RH700 are reconstructed from the individual climate modes for each year, and

418   then we calculate spatial correlations between the observed anomalies (e.g., left panels in Figs.

419   10 and 11) and model-reconstructed anomalies corresponding to each mode (see Table 3). The

420   results reveal a prominent role of the AMM in 2005. In fact, the correlations with observation are

421   highest for all four variables when the AMM is considered for reconstruction (see 3–6th rows

422   and 3–6th columns in Table 3). Specifically, favorable conditions for TC genesis and tracks over

423   the western Atlantic and Gulf of Mexico resulting from strong negative SLP (Fig. 10a),

424   weakening of westerly shear (Fig. 11a), and positive humidity (Fig. 11a) anomalies can be

425   largely linked to the positive SSTs caused by a strong positive AMM over that region. The

426   atmospheric anomalies forced by the tropical eastern Pacific SST, which was almost bordering

427   near-neutral ENSO conditions (see Fig. 6d), show a negative or weak positive correlation with

428   the observations (3rd row and 3–6th columns in Table 3), suggesting that the ENSO impact is

429   overwhelmed by the strong positive AMM. This relative influence of ENSO and AMM appears

430   very important to explain seasonal Atlantic TC activity (Patricola et al. 2014).

431   The ENSO signal (El Niño) in 2006 (Fig. 6d) is more important in characterizing the

432   atmospheric anomalies than in 2005. However, since the 2006 El Niño was not a strong event,

433   its impact does not stand out among the three modes in accounting for the seasonal atmospheric

434   patterns during that year (7–10th rows and 3–6th columns in Table 3). We can speculate that the

435   TC activity during 2006 can be understood as the combined effect of the weak El Niño, neutral

436   NAO, and neutral AMM in summer, and possibly other forcings not included in this work such

437   as unusual dust activity (Lau and Kim 2007).

438   The active hurricane season of 2010 is found to be significantly correlated with ENSO and

439   the AMM. All four variables constructed from La Niña (Fig. 6d) or the positive AMM (Fig. 6f)

19

440   are more highly correlated with the observations than the negative NAO. However, the negative

441   phase of the NAO exerts some control on the TC track patterns, which are very different from

442   the other active TC season of 2005. While the impact of the strong positive AMM phase is

443   comparable in 2005 and 2010, Fig. 12 shows that the impact of the ENSO and NAO modes is

444   drastically different. Fig. 12a suggests that the neutral ENSO and positive NAO in 2005 produce

445   weak positive SLP anomalies over the Atlantic, notwithstanding a substantial positive AMM-

446   induced modification in 2005. In contrast, the impacts of the La Niña and negative NAO in 2010

447   produce negative SLP anomalies (Fig. 12b) and positive SST anomalies (Figs. 12d) over the

448   entire subtropical Atlantic. This impact, combined with the positive AMM, further enhances the

449   negative SLP and positive SST anomalies over the subtropical Atlantic. The above differences in

450   the climate anomalies may explain why TC genesis was mainly confined to the western Atlantic

451   in 2005, with very few Cape Verde systems, in contrast with 2010.

452   Correlations for the 2013 hurricane season indicate a significant contribution of the NAO to

453   the observed anomaly distributions. While the other two modes were weak in magnitude, the

454   impact of the positive NAO (known to weaken TC genesis over the North Atlantic - Knaff

455   (1997) and Kossin et al. (2010)) appeared to exert strong control in developing conditions

456   unfavorable   to   TC   activity   (see   also

457   http://www.srh.noaa.gov/bro/?n=2013event_hurricaneseasonwrap). Table 3 shows that the

458   correlations between observations and the reconstructed variables based on the NAO are greatest

459   (15–18th rows and 3–6th columns in Table 3) without exception, with the other two modes

460   having much lower correlations with observations. This argument appears connected with Zhang

461   et al. (2016) that suggested the role of strong anti-cyclonic Rossby wave breaking, which tends

462   to be more active during the positive NAO phase (Riviére et al. 2010) and could have

463 contributed to equatorward intrusion of extratropical dry air especially in August and September

464 in 2013, leading to poor conditions for TC activity.

465   Consistent with previous findings, the NR results are relatively poor when compared to the

466 R8W (3rd–6th vs 7–10th columns in Table 3). Although the NR run is successful in reproducing

467 the interannual variation of the TC genesis frequency, it is not so successful in reproducing the

468 spatial structure of the three dominant modes, their interannual variation of phase and intensity,

469 and the associated seasonal TC track patterns for each year.

470

471 3.6 TC genesis frequency statistics associated with the MJO

472   An additional question addressed in this section is whether the simulations that constrain the

473 atmospheric planetary-scales larger than ~5,000 km wavelength (corresponding to R8W) can

474 realistically capture the Atlantic TC genesis frequency statistics, known to depend on the phase

475 of the MJO (Maloney and Hartmann 2000; Camargo et al. 2009; Kossin et al. 2010; Klotzbach

476 2010). To this purpose, the timing of the TC genesis associated with the phase of MJO is

477 examined by counting the TC genesis dates from observations, R5W run, and R8W run with

478 respect to the MJO phases using the Wheeler and Hendon (2004) MJO indices. The

479 observationally-based results (Table 4) reveal that TC genesis tends to be most active when the

480 MJO-enhanced convection with tropical westerlies occurs in the western hemisphere (phase 1

481 and 8, Wheeler and Hendon 2004), while TC genesis becomes inactive when the MJO-enhanced

482 convection occurs over the western Pacific (phase 6 and 7), consistent with Maloney and

483 Hartmann (2000) and Klotzbach and Oliver (2015). This characteristic feature of the MJO is

484 reproduced better in R8W than in R5W, demonstrating that atmospheric scales between 8000km

485 and 5000km are very important to realistically explain the TC genesis frequency statistics

486   associated with the MJO phase.

487

488   3.7 Predicting the large-scale impacts of ENSO, NAO, and AMM

489   The previous results consistently indicate that the unconstrained NR cannot reproduce the

490   planetary scale atmospheric features important for TC seasonal prediction. In this section, the

491   issue of SST-based predictability of relevant atmospheric variations associated with the three

492   leading modes (ENSO, NAO, and AMM) is investigated with the aid of the GEOS-5 AGCM

493   forced with observed SSTs. To this purpose, an ensemble of twenty NRs was produced for each

494   of the nine TC seasons (2005-2013). The ensemble members differ only in the atmospheric/land

495   initial conditions taken from MERRA for May 1 to May 20 of each year. The predictability of

496   the individual modes is assessed in terms of signal to noise (S/N) ratios for SLP and z250. The

497   SLP and z250 distributions associated with the ENSO, NAO, and AMM modes are identified

498   and then the interannual variations of these modes are examined for each ensemble member.

499   The left panel in Fig. 13 shows the z250 anomalies associated with the three modes,

500   respectively. The light-green contours are the results for each ensemble member. The results

501   show considerable scatter among the members, especially over mid-latitude region (say north of

502   25°N). The ensemble mean anomalies represented by black contours do, however, resemble the

503   typical observed z250 anomaly distributions associated with the positive phase of the ENSO,

504   NAO, and AMM modes (cf. Figs. 13a,b,c with Figs. 7d,8d,9d). However, the PC time series

505   shown in the right panel of Fig. 13 reveal large uncertainty in the interannual variation of the

506   phase of the ENSO and NAO modes. This large ensemble spread indicates that predictability of

507   these two major modes of variability impacting TC activity is low on seasonal time scales in

508   summer, though we cannot rule out the possibility that this reflects model errors. Particularly, the

509　large uncertainty associated with ENSO seems to be due to inconsistent extra-tropical responses

510　to the ENSO forcing among the members. The uncertainty is significantly reduced when we

511　focus on the tropical region only (e.g., tropical Atlantic and eastern Pacific) for capturing the

512　ENSO mode (Figure not shown) (see also high S/N ratios over the tropics in Figs. 14a,d).

513　Compared to ENSO and the NAO, the predictability of the AMM is considerably higher as all

514　ensemble members exhibit similar variations, in good agreement with the observed values (Fig.

515　13f).

516　　　The distribution of the S/N ratio of the monthly variation of the ENSO, NAO, and AMM

517　modes is shown in Fig. 14. The S/N ratio increases with a decrease in variance of intra-ensemble

518　differences (i.e., residual variance). The S/N ratios for ENSO reveal that the highest SLP S/N

519　ratio is found over the eastern tropical Pacific. The low-latitudes of the Atlantic region exhibit

520　the second highest S/N ratios. This includes the Gulf of Mexico, part of the Caribbean Sea and

521　the eastern subtropical Atlantic, where many TCs are typically generated. The predictability of

522　z250 associated with the ENSO signal is high (> 0.8) over the low-latitude Atlantic basin. The

523　Caribbean Sea region has the largest S/N ratio, exceeding 0.9 (Fig. 14d).

524　　　The predictability of the NAO-related response is found to be relatively low. Figure 14b

525　shows that the highest S/N ratios for SLP are limited to the eastern tropical Pacific and the

526　Caribbean Sea. The S/N ratios for z250 suggest that relatively high predictability occurs in a belt

527　confined to ~20°N (Fig. 14e), with S/N values in other regions between zero and 0.2.

528　　　The predictability of the AMM represented by z250 is found to be higher than the one

529　associated with ENSO over low-latitudes (compare Figs. 14d,f). Figure 14f shows that the S/N

530　ratio is close to 1 within +/- 20° of the equator. However, the S/N ratio drops rapidly to values

531　smaller than 0.2 to the north of 40°N. The predictability of the AMM in terms of SLP is higher

532   over the tropical eastern Pacific and the western Atlantic including the Caribbean Sea (Fig. 14c).

533   Figures 13 and 14 suggest that predictive skill of the primary large-scale modes of

534   variability of the atmosphere is to a large extent limited to the tropical to sub-tropical regions.

535   This is particularly true for the NAO. Whether this represents a realistic estimate of intrinsic

536   atmospheric predictability on seasonal time scales (linked to SST), or whether this partly reflects

537   a limitation of the GEOS-5 AGCM is yet to be determined. Extra-tropical weather patterns,

538   affected by transient dynamical forcings which have generally larger amplitudes than the tropical

539   ones, may contribute to the relatively low NAO predictability. It is likely that the extra-tropical

540   North Atlantic region, dominated by baroclinic activity, needs additional investigation to

541   improve prediction of the largest planetary-scales.

542

543   4. Concluding remarks and discussion

544   This study examined the impact of the large-scale climate modes on seasonal Atlantic TC

545   activity by focusing on genesis frequency, genesis locations, and overall track patterns and

546   landfalls. A particular focus was on the unexpected TC activity that occurred in recent several

547   years (e.g., 2005, 2006, 2010 and 2013). Both observational analysis and climate model

548   simulations were conducted to better understand the large-scale climate modes that impact

549   Atlantic TC activity on seasonal time scales. Three leading well-known climate modes were

550   identified consisting of ENSO, the NAO and the AMM. It was found that a substantial amount

551   of the variability in the observed mass fields (SLP and upper-level geopotential height (z250)),

552   vertical wind shear, and relative humidity over the North Atlantic can be reproduced as a linear

553   combination of these three modes, highlighting the important role they play in impacting year-to-

554   year changes in seasonal TC activity.

555   In spite of the general relationship between the Atlantic TC genesis frequency and ENSO

556   (Bove et al. 1998; Elsner and Bossak 2001; Klotzbach 2011), there have been several years with

557   active TC genesis during the warm ENSO and inactive TC genesis during cold ENSO. In this

558   study, it was suggested that the counter-intuitive TC activity that occurred in 2005 and 2013 is

559   the result of the strong impact of a positive AMM in 2005 and a positive NAO in 2013, which

560   acted to modify the impact of ENSO. A positive AMM caused warmer SSTs to occur over the

561   western and central Atlantic in 2005, leading to more favorable conditions for active TC genesis

562   in that region compared to that in the eastern Atlantic, and more landfalls over the US. For the

563   case of a weak TC season in 2013, the strong impact of a positive NAO overwhelmed a weak

564   negative Niño SST impact, producing a positive SLP anomaly over the Atlantic, stronger vertical

565   westerly shear, and drier atmosphere (~700hPa) over the Atlantic TC genesis region. As such,

566   this year was strongly impacted by the extratropics, unlike the other years that were primarily

567   controlled by the changes in the low-latitude Atlantic (e.g., tropical SST).

568   For the case of 2010, widespread negative SLP anomalies occurred over the subtropical

569   Atlantic due to the combined influence of La Niña, a negative NAO and a positive AMM,

570   providing very favorable conditions for TC genesis over that region. The impact of the three

571   modes was to also produce an expanded area of positive SST anomalies across the low-latitudes

572   of the Atlantic and a weak westward expansion of the North Atlantic subtropical high, leading to

573   more early recurvers and fewer landfalling systems over the US, despite it being an active TC

574   year. The 2006 TC season also appears to be controlled by a synergy of the three modes in

575   producing the seasonal atmospheric anomalies that drove the weak TC activity. Additionally, a

576   TC-suppressing role attributed by other authors to anomalous dust production and reduced SSTs

577   in 2006 (Lau and Kim 2007), not investigated in this work, should be taken into account.

578   This study also found that, in general, the large-scale atmospheric variability over the

579   subtropical North Atlantic with wavelengths approximately greater than 4,000–5,000km, which

580   is much larger than the typical horizontal scale of TCs, is responsible for controlling the changes

581   in North Atlantic TC activity on seasonal time scales. In fact, those scales are sufficient to

582   faithfully account for the relevant spatio-temporal variations of ENSO, the NAO, and the AMM.

583   Our analysis reveals that the seasonal atmospheric anomalies during any particular year are very

584   sensitive to the phase and intensity of these modes. As such, the combined impact of these modes

585   can produce seasonal TC activity that is opposite to the conventional understanding about the

586   impact of any of the leading modes alone (e.g., strong TC activity during a neutral ENSO and

587   positive NAO in 2005, and weak TC activity during weak negative Niño index in 2013). This

588   study suggests that while ENSO is very important, its interaction with the AMM and NAO (and

589   perhaps other forcings) in modulating the Atlantic TCs appears to provide a more robust

590   explanation of TC interannual variability.

591   A caveat for this study is that the impact of the Atlantic Multi-decadal Oscillation (AMO)

592   (Klotzbach 2011; Caron et al. 2014), also known to be important for influencing Atlantic TC

593   activity on decadal time scales (a positive AMO, characterized by positive Atlantic SST

594   anomalies, is associated with more intense hurricanes), is not included in this work. Vimont and

595   Kossin (2007) suggest that the impact of the AMO on seasonal TC activity manifests itself

596   through the AMM because the AMO can excite the AMM on decadal time scales. The AMO has

597   been in the positive phase for our analysis period (2005-2013), thus possibly enhancing Atlantic

598   TC activity. However, the AMO index was only slightly positive during the late spring in 2013.

599   Fogarty and Klotzbach (2014) suggest that AMO weakening on subseasonal time scale might

600   have a delayed TC suppressing impact in 2013, interacting with the extra-tropical impact by the

26

601   positive phase of the NAO.

602   This study contributes to the understanding of TC predictability on seasonal and subseasonal

603   scales by showing evidence that phase and intensity of the AMM are more predictable, followed

604   by ENSO, particularly over low latitudes. The predictive skill for both modes declines towards

605   the mid latitudes, where the response to the AMM or ENSO tends to be inconsistent among

606   different ensemble members, implying larger uncertainty. An even more challenging aspect of

607   the TC prediction problem is the relatively low predictability of NAO because of its intrinsically

608   shorter time scales and greater association with the mid-latitude dynamics. As a future and

609   challenging step towards increased TC predictability on a subseasonal scale, inclusive of track

610   and landfall distributions, a more advanced understanding of the NAO will be necessary.

611

612   Acknowledgements

616   References

617   Aiyyer, A. R., and C. Thorncroft, 2006: Climatology of vertical wind shear over the tropical
618   Atlantic. *J. Climate*, **19**, 2969-2983.

619   Barnston, A. G., and R. E. Livezey, 1987: Classification, seasonality and persistence of low-
620   frequency atmospheric circulation pattern. *Mon. Wea. Rev*., **115**, 1083-1126.

621   Bacmeister, J. T., M. J. Suarez, and F. R. Robertson, 2006: Rain reevaporation, boundary layer–
622   convection interactions, and Pacific rainfall patterns in an AGCM. *J. Atmos. Sci.*, **63**, 3383–
623   3403.

624   Bacmeister, J. T., M. F. Wehner, R. B. Neale, A. Gettelman, C. Hannay, P. H. Lauritzen, J. M.
625   Caron, and J. E. Truesdale, 2014: Exploratory high-resolution climate simulations using the
626   Community Atmosphere Model (CAM). *J. Climate*, **27**, 3073-3099.

627   Bell, G. D., E. S. Blake, T. B. Kimberlain, C. W. Landsea, J.-K. E. Schemm, R. J. Pasch, and S.
628   B. Goldenberg, 2011: State of the climate 2010. *Bull. Amer. Meteor. Soc.,* **92(6)**, S115-120.

629   Blake E. S., and E. J. Gibney, 2011: The deadliest, the costliest, and most intense United States
630   tropical cyclones from 1851 to 2010 (and other frequently requested hurricane facts). NOAA
631   Technical Memorandum NWS NHC-6, 47pp.

632   Blake, E. S., National Hurricane Center Annual Summary. 2013 Atlantic Hurricane Season, 9pp.
633   Available at http://www.nhc.noaa.gov/data/tcr/summary_atlc_2013.pdf

634   Bloom, S., L. Takacs, A. DaSilva, and D. Ledvina, 1996: Data assimilation using incremental
635   analysis updates. *Mon. Wea. Rev*., **124**, 1256-1271.

636   Bove, M. C., J. J. O'Brien, J. B. Eisner, C. W. Landsea, and X. Niu, 1998: Effect of El Niño on
637   U.S. landfalling hurricanes, revisited. *Bull. Amer. Meteor. Soc.*, **79**, 2477–2482.

638   Camargo, S. J., K. Emanuel, and A. Sobel, 2007: Use of a genesis potential index to diagnose
639   ENSO effects on tropical cyclone genesis. *J. Climate*, **20**, 4819-4834.

640   Camargo, S. J., M. C. Wheeler, and A. H. Sobel, 2009: Diagnosis of the MJO modulation of
641   tropical cyclogenesis using and empirical index. *J. Atmos. Sci*., **66**, 3061-3074, doi:
642   10.1175/2009JAS3101.1.

643   Caron, L.-P., M. Boudreault, and C. L. Bruyère, 2014: Changes in large-scale controls of
644   Atlantic tropical cyclone activity with the phases of the Atlantic multidecadal oscillation.
645   *Clim. Dyn*., doi: 10.1007/s00382-014-2186-5.

646 Chen, J.-H., and S.-J. Lin, 2013: Seasonal Predictions of Tropical Cyclones Using a 25-km
647   Resolution General Circulation Model. *J. Climate*, **26**, 380-398, doi:10.1175/JCLI-D-12-
648   00061.1.

649 Chiang, J. C. H., and D. J. Vimont, 2004: Analagous meridional modes of atmosphere-ocean
650   variability in the tropical Pacific and tropical Atlantic. *J. Climate*, **17**, 4143-4158.

651 Colbert, A. J., and B. J. Soden, 2012: Climatological variations in North Atlantic tropical
652   cyclone tracks. *J. Climate*, **25**, 657-673, doi: 10.1175/JCLI-D-11-00034.1.

653 Deser, C., M. A. Alexander, S.-P. Xie, and A. S. Phillips, 2010: Sea surface temperature
654   variability: Patterns and mechanisms. *Annu. Rev. Mar. Sci.*, 115-143.

655 Elsner, J. B., and B. H. Bossak, 2001: Secular changes to the ENSO-U.S. hurricane relationship.
656   *Geophys. Res. Lett.*, **28(21)**, 4123-4126.

657 Elsner, J. B., 2003: Tracking hurricanes. *Bull. Amer. Meteor. Soc.*, **84**, 353–356.

658 Elsner, J. B., and T. Jagger, 2006: Prediction models for annual US Hurriane counts. *J. Climate,*
659   **19,** 2935-2952.

660 Fogarty, C. T., and P. Klotzbach, 2014: The 2013 Atlantic hurricane season: blip or flip? *Bull.*
661   *Amer. Meteor. Soc.*, **95(7)**, S106-107.

662 Gelaro, R., and co-authors, 2015: *Evaluation of the 7-km GEOS-5 Nature Run*. NASA Technical
663   Report Series on Global Modeling and Data Assimilation, NASA/TM-2014-104606, **36**. 305
664   pp.

665 Knaff, J. A., 1997: Implications of summertime sea level pressure anomalies in the tropical
666   Atlantic region. *J. Climate*, **10**, 789–804.

667 Kim, H.-M., and P. J. Webster, 2010: Extended-range seasonal hurricane forecasts for the North
668   Atlantic with a hybrid dynamical-statistical model. Geophys. Res. Lett., 37, L21705,
669   doi:10.1029/2010GL044792.

670 Klotzbach, P. J., and W. M. Gray, 2004: Updated 6-11-month prediction of Atlantic basin
671   seasonal hurricane activity. *Wea. Forecasting*, **19**, 917-934.

672 Klotzbach, P. J., 2010: On the Madden-Julian Oscillation-Atlantic hurricane relationship. *J.*
673   *Climate*, **23**, 282-293, doi: 10.1175/2009JCLI2978.1.

674 Klotzbach, P. J., 2011: The influence of El Niño-Southern Oscillation and the Atlantic
675   multidecadal oscillation on Caribbean tropical cyclone activity. *J. Climate*, **24**, 721-731, doi:
676   10.1175/2010JCLI3705.1.

677 Klotzbach, P. J., and E. C. J. Oliver, 2015: Modulation of the Atlantic basin tropical cyclone

678   activity by the Madden-Julian Oscillation (MJO) from 1905 to 2011. *J. Climate*, **28**, 204-217,

679   doi: 10.1175/JCLI-D-14-00509.1.

680 Knutson, T. R., J. J. Sirutis, S. T. Garner, I. M. Held, and R. E. Tuleya, 2007: Simulation of the

681   recent multidecadal increase of Atlantic hurricane activity using an 18-km-grid regional

682   model. B*ull. Amer. Meteor. Soc.*, **88**, 1549–1565.

683 Kossin, J. P., and D. J. Vimont, 2007: A more general framework for understanding Atlantic

684   hurricane variability and trends. *Bull. Amer. Meteor. Soc.*, **88**, 1767-1781.

685 Kossin, J. P., and S. J. Camargo, 2009: Hurricane track variability and secular potential intensity

686   trends. *Climate Change*, **97**, 329-337, doi:10.1007/s10584-009-9748-2.

687 Kossin, J. P., S. J. Camargo, and M. Sitkowski, 2010: Climate modulation of North Atlantic

688   hurricane tracks. *J. Climate*, **23**, 3057-3076.

689 Koster, R. D., M. J. Suarez, A. Ducharne, M. Stieglitz, and P. Kumar, 2000: A catchment-based

690   approach to modeling land surface processes in a general circulation model: 1. Model

691   structure. *J. Geophys. Res.*, **105**, 24809–24822, doi:10.1029/2000JD900327.

692 Landsea, C. W., and J. L. Franklin, 2013: Atlantic hurricane database uncertainty and

693   presentation of a new database format. *Mon. Wea. Rev*., **141**, 3576-3592, doi:

694   10.1175/MWR-D-12-00254.1.

695 LaRow, T. E., Y.-K. Lim, D. W. Shin, S. Cocke, and E. P. Chassignet, 2008: Atlantic basin

696   seasonal hurricane simulations. *J. Climate*, **21**, 3191-3206, doi:10.1175/2007JCLI2036.1.

697 Larson, J., Y. Zhou, and R. W. Higgins, 2005: Characteristics of landfalling tropical cyclones in

698   the United States and Mexico: Climatology and interannual variability. *J. Climate*, **18**,

699   1247–1262.

700 Lau, K.-M., and K. M. Kim, 2007: Cooling of the Atlantic by Saharan dust. *Geophys. Res. Lett*.,

701   **34**, L23811, doi:10.1029/2007GL031538.

702 Lim, Y.-K., S. D. Schubert, O. Reales, M.-Y. Lee, A. M. Molod, and M. J. Suarez,

703   2015: Sensitivity of tropical cyclones to parameterized convection in the NASA GEOS5

704   model. *J. Climate*, **28(2)**, 551-573, doi:10.1175/JCLI-D-14-00104.1.

705 Lin, S.-J., 2004: A vertically Lagrangian finite-volume dynamical core for global models. *Mon.*

706   *Wea. Rev.*, **132**, 2293–2307.

707 Maloney, E. D., and D. L. Hartmann, 2000: Modulation of hurricane activity in the Gulf of
708   Mexico by the Madden-Julian Oscillation. *Science*, **287**, 2002-2004.

709 Mo, K. C., 2000: The association between intraseasonal oscillations and tropical storms in the
710   Atlantic basin. *Mon. Wea. Rev*., **128**, 4097-4107.

711 Molod, A., L. Takacs, M. Suarez, J. Bacmeister, I.-S. Song, and A. Eichmann, 2012: The GEOS-
712   5 Atmospheric General Circulation Model: Mean Climate and Development from MERRA
713   to Fortuna. *NASA Technical Report Series on Global Modeling and Data Assimilation,*
714   *NASA TM—2012-104606*, **28**, 117 pp.

715 Moorthi, S., and M. J. Suarez, 1992: Relaxed Arakawa-Schubert: A parameterization of moist
716   convection for general circulation models. *Mon. Wea. Rev*., **120**, 978-1002.

717 Murakami, H., G. A. Vecchi, S. Underwood, T. L. Delworth, A. T. Wittenberg, W. G. Anderson,
718   J.-H. Chen, R. G. Gudgel, L. M. Harris, S.-J. Lin, and F. Zeng, 2015: Simulation and
719   prediction of category 4 and 5 hurricanes in the high-resolution GFDL HiFLOR coupled
720   climate model. *J. Climate*, **28**, 9058-9079, doi: 10.1175/JCLI-D-15-0216.1.

721 O'Brien, J. J., T. S. Richards, and A. C. Davies, 1996: The effect of El Niño on U.S. landfalling
722   hurricanes. *Bull. Amer. Meteor. Soc*. **77**, 773-774.

723 Patricola, C. M., R. Saravanan, and P. Chang, 2014: The impact of the El Niño-Southern
724   Oscillation and Atlantic meridional mode on seasonal Atlantic tropical cyclone activity. J.
725   Climate, 5311-5328, doi: 10.1175/JCLI-D-13-00687.1.

726 Putman, W. M., and M. Suarez. 2011: Cloud-system resolving simulations with the NASA
727   Goddard Earth Observing System global atmospheric model (GEOS-5). *Geophys. Res. Lett*.,
728   **38(16)**, L16809, doi:10.1029/2011GL048438.

729 Rayner, N. A., and Coauthors, 2003: Global analyses of sea surface temperature, sea ice, and
730   night time air temperature since the late nineteenth century. *J. Geophys. Res*., **108,** (D14),
731   4407, doi:10.1029/2002JD002670.

732 Reale, O., W. K. Lau, J. Susskind, E. Brin, E. Liu, L. P. Riishojgaard, M. Fuentes, and R.
733   Rosenberg, 2009: AIRS impact on the analysis and forecast track of tropical cyclone Nargis
734   in a global data assimilation and forecasting system. *Geophys. Res. Lett*., **36**, L06812,
735   doi:10.1029/2008GL037122.

736 Reed, K. A., and C. Jablonowski, 2011: Impact of physical parameterizations on idealized
737   tropical cyclones in the Community Atmosphere Model. *Geophys. Res. Lett.*, **38**, L04805,
738   doi:10.1029/2010GL046297.

739 Rienecker M. M. and Coauthors, 2008: The GEOS-5 data assimilation system – documentation
740   of versions 5.0.1 and 5.1.0, and 5.2.0. In: NASA technical report series on global modeling
741   and assimilation, NASA/TM-2008-104606, **27**, 92pp.

742 Rienecker, M.M., and Coauthors, 2011: MERRA - NASA's Modern-Era Retrospective Analysis
743   for Research and Applications. *J. Climate*, **24**, 3624-3648. doi: 10.1175/JCLI-D-11-00015.1.

744 Rivière, G., A. Laîné, G. Lapeyre, D. Salas-Mélia, and M. Kageyama, 2010: Links between
745   Rossby wave breaking and the North Atlantic oscillation–Arctic oscillation in present-day
746   and last glacial maximum climate simulations. *J. Climate*, **23**, 2987–3008,
747   doi:10.1175/2010JCLI3372.1.

748 Shaman, J., S. K. Esbensen, and E. D. Maloney, 2009: The dynamics of the ENSO-Atlantic
749   hurricane teleconnection: ENSO-related changes to the North African-Asian jet affect
750   Atlantic basin tropical cyclogenesis. *J. Climate*, **22**, 2458-2482.

751 Smirnov, D., and D. J. Vimont, 2011: Variability of the Atlantic meridional mode during the
752   Atlantic hurricane season. *J. Climate*, **24**, 1409-1424, doi: 10.1175/2010JCLI3549.1.

753 Smith, S. R., J. Brolley, J. J. O'Brien, and C. A. Tartaglione, 2007: ENSO's impact on regional
754   U.S. hurricane activity. *J. Climate*, **20**, 1404–1414.

755 Tartaglione, C. A., S. R. Smith, and J. J. O'Brien, 2003: ENSO impact on hurricane landfall
756   probabilities for the Caribbean. *J. Climate*, **16**, 2925–2931.

757 Tokioka, T., K. Yamazaki, A. Kitoh, and T. Ose, 1988: The equatorial 30–60 day oscillation and
758   the Arakawa-Schubert penetrative cumulus parameterization, *J. Meteorol. Soc. Japan.*, **66**,
759   883–901.

760 Vecchi, G. A., and coauthors, 2014: On the seasonal forecasting of regional tropical cyclone
761   activity. *J. Climate*, **27**, 7994-8016, doi: 10.1175/JCLI-D-14-00158.1.

762 Vimont, D. J., and J. P. Kossin, 2007: The Atlantic meridional mode and hurricane activity.
763   *Geophys. Res. Lett.*, **34**, L07709, doi: 10.1029/2007GL029683.

764 Vitart, F., D. Anderson, and T. Stockdale, 2003: Seasonal forecasting of tropical cyclone landfall
765   over Mozambique. *J. Climate*, **16**, 3932-3945.

766 Wallace, J. M., and D. S. Gutzler, 1981: Teleconnections in the geopotential height field during
767   the Northern Hemisphere winter. *Mon. Wea. Rev.*, **109**, 784–812.

768 Walsh, K. J. E., M. Fiorino, C. W. Landsea, and K. L. McInnes, 2007: Objectively determined
769   resolution-dependent threshold criteria for the detection of tropical cyclones in climate
770   models and reanalyses. *J. Climate,* **20**, 2307–2314.

771 Wang, C., H. Liu, S.-K. Lee, and R. Atlas, 2011: Impact of the Atlantic warm pool on United
772   States landfalling hurricanes. *Geophys. Res. Lett.*, **38**, L19702, doi:10.1029/2011GL049265.

773 Wang, Z., G. Zhang, M. S. Peng, J.-H. Chen, and S.-J. Lin, 2015: Predictability of Atlantic
774   Tropical Cyclones in the GFDL HiRAM Model. *Geophys. Res. Lett.*, **42(7)**,
775   doi:10.1002/2015GL063587.

776 Wheeler, M. C., and H. H. Hendon, 2004: An all-season real-time multivariate MJO index:
777   Development of an index for monitoring and prediction. *Mon. Wea. Rev.*, **132**, 1917-1932.

778 Xie, L., T. Yan, L. J. Pietrafesa, J. M. Morrison, and T. Karl, 2005: Climatology and interannual
779   variability of North Atlantic hurricane tracks. *J. Climate*, **18**, 5370-5381.

780 Zhang, G., Z. Wang, T. Dunkerton, M. Peng, and G. Magnusdottir, 2016: Extratropical impacts
781   on Atlantic tropical cyclone activity. *J. Atmos. Sci*, in press.

782 Zhao, M., I. M. Held, S.-J. Lin, and G. A. Vecchi, 2009: Simulations of global hurricane
783   climatology, interannual variability, and response to global warming using a 50-km
784   resolution GCM. *J. Climate*, **22**, 6653-6678, doi:10.1175/2009JCLI3049.1.

785 Zhao, M., I. M. Held, and S.-J. Lin, 2012: Some counter-intuitive dependencies of tropical
786   cyclone frequency on parameters in a GCM. *J. Atmos. Sci.*, **69(7)**, 2272-2283,
787   doi:10.1175/JAS-D-11-0238.1.

788 Zhu, X., R. Saravanan, and P. Chang, 2012: Influence of mean flow on the ENSO-vertical wind
789   shear relationship over the northern tropical Atlantic. J. Climate, 25, 858-864, doi:
790   10.1175/JCLI-D-11-00213.1.

791   **Table 1**. List of the threshold values for detecting the TC using the detection/tracking algorithm
792   based on Vitart et al. (2003)

Variables	local relative vorticity maximum (850hPa)	warm core temperature maximum	minimum sea level pressure (SLP)	minimum lower-level wind speed	minimum duration
Criteria	3.5×10^{-5} s^{-1}	Distance between the TC center and the center of the warm core must not exceed 2° lon.&lat.	Minimum SLP defines the TC center and must exist within 2°×2° radius of the vorticity maximum	12m s^{-1}	2 days

793

794   **Table 2**. TC track density and the number of TC landfalls (numbers in parentheses) averaged
795   over the continental 1) US and Canada, and 2) Mexico and Central America. Results from
796   observations are shown in the third column, while three ensemble member mean results for R5W,
797   R8W, and NR, respectively, are shown in 4–6th columns. TC track density and landfalling TC
798   counts are calculated for each hurricane season (2005, 2006, 2010, and 2013).

		TC track density (landfalls)			
		Obs.	R5W	R8W	NR
2005	US and Canada	0.58 (6)	0.49 (4.7)	0.54 (5)	0.36 (3.7)
	Mexico and Central America	1.27 (5)	0.69 (1)	1.28 (1.7)	1.18 (2)
2006	US and Canada	0.26 (2)	0.18 (2.7)	0.20 (1.7)	0.25 (3.3)
	Mexico and Central America	0.0 (0)	0.39 (0.3)	0.37 (0.7)	0.53 (1.7)
2010	US and Canada	0.13 (2)	0.18 (2.7)	0.16 (1.7)	0.47 (5.3)
	Mexico and Central America	1.26 (6)	1.63 (2.7)	1.09 (3)	1.71 (4)
2013	US and Canada	0.25 (1)	0.16 (1.3)	0.09 (2)	0.35 (3.7)
	Mexico and Central America	1.13 (2)	0.33 (0.7)	0.47 (1.7)	0.73 (2)

799

Table 3. Spatial correlations between observed anomaly distribution (left panels in Figs. 10 and 11) and distribution of reconstructed model-anomalies associated with the phase and intensity of the ENSO, NAO, and AMM, respectively. Spatial correlations are calculated for each hurricane season (2005, 2006, 2010, and 2013). The observed phases of each leading mode in each year are noted within parentheses in the second column. Variables considered for examining spatial correlations are SLP, z250, vertical wind shear (WS), and 700hPa relative humidity (RH).

		Obs. vs. R8W				Obs. vs. NR			
		SLP	z250	WS	RH	SLP	z250	WS	RH
2005	ENSO (0)	-0.02	-0.36	0.28	-0.02	-0.02	-0.06	0.01	0.27
	NAO (+)	0.43	0.34	0.06	0.18	-0.22	-0.37	0.05	-0.39
	AMM (+)	0.79	0.63	0.56	0.49	0.57	0.03	0.47	0.59
	E+N+A	0.71	0.63	0.56	0.50	0.20	0.01	0.42	0.59
2006	ENSO (+)	0.54	0.34	0.30	0.02	-0.09	0.63	0.35	0.07
	NAO (0)	0.30	0.58	0.26	0.01	0.10	0.48	0.25	0.11
	AMM (0)	0.58	0.19	0.39	0.03	0.63	-0.16	0.38	0.00
	E+N+A	0.70	0.45	0.35	0.01	0.10	0.61	0.48	0.08
2010	ENSO (–)	0.74	0.64	0.56	0.29	0.44	0.77	0.65	0.32
	NAO (–)	0.20	0.16	0.27	-0.06	0.23	0.22	0.39	0.31
	AMM (+)	0.58	0.78	0.71	0.46	0.30	-0.17	0.74	0.18
	E+N+A	0.86	0.88	0.92	0.51	0.41	0.34	0.79	0.40
2013	ENSO (0)	0.13	0.01	0.14	0.12	-0.18	-0.12	-0.47	-0.01
	NAO (+)	0.82	0.32	0.54	0.43	0.43	0.13	0.64	0.09
	AMM (+)	0.26	0.23	0.55	0.10	0.75	0.44	0.63	0.14
	E+N+A	0.85	0.31	0.46	0.15	0.40	-0.02	-0.14	0.04

Table 4 The number of TC genesis within different MJO phases (Wheeler and Hendon 2004). Phase 2 and 3, phase 4 and 5, phase 6 and 7, and phase 8 and 1 represents, respectively, the MJO-driven convection over the Indian Ocean, the Maritime Continents, the western North Pacific, and the western Hemisphere. Note that the number of TC genesis obtained from the R5W and the R8W data are the sum of all TCs in the three ensemble members.

	Phase 2 and 3	Phase 4 and 5	Phase 6 and 7	Phase 8 and 1
Obs.	17	17	8	25
R5W	53	45	26	52
R8W	58	45	21	67

Figure Captions

Figure 1. A schematic view of replaying the GEOS-5 model to an existing atmospheric analysis dataset. The process is generalized here to apply a filter to the full increments to allow constraining a subset of the flow.
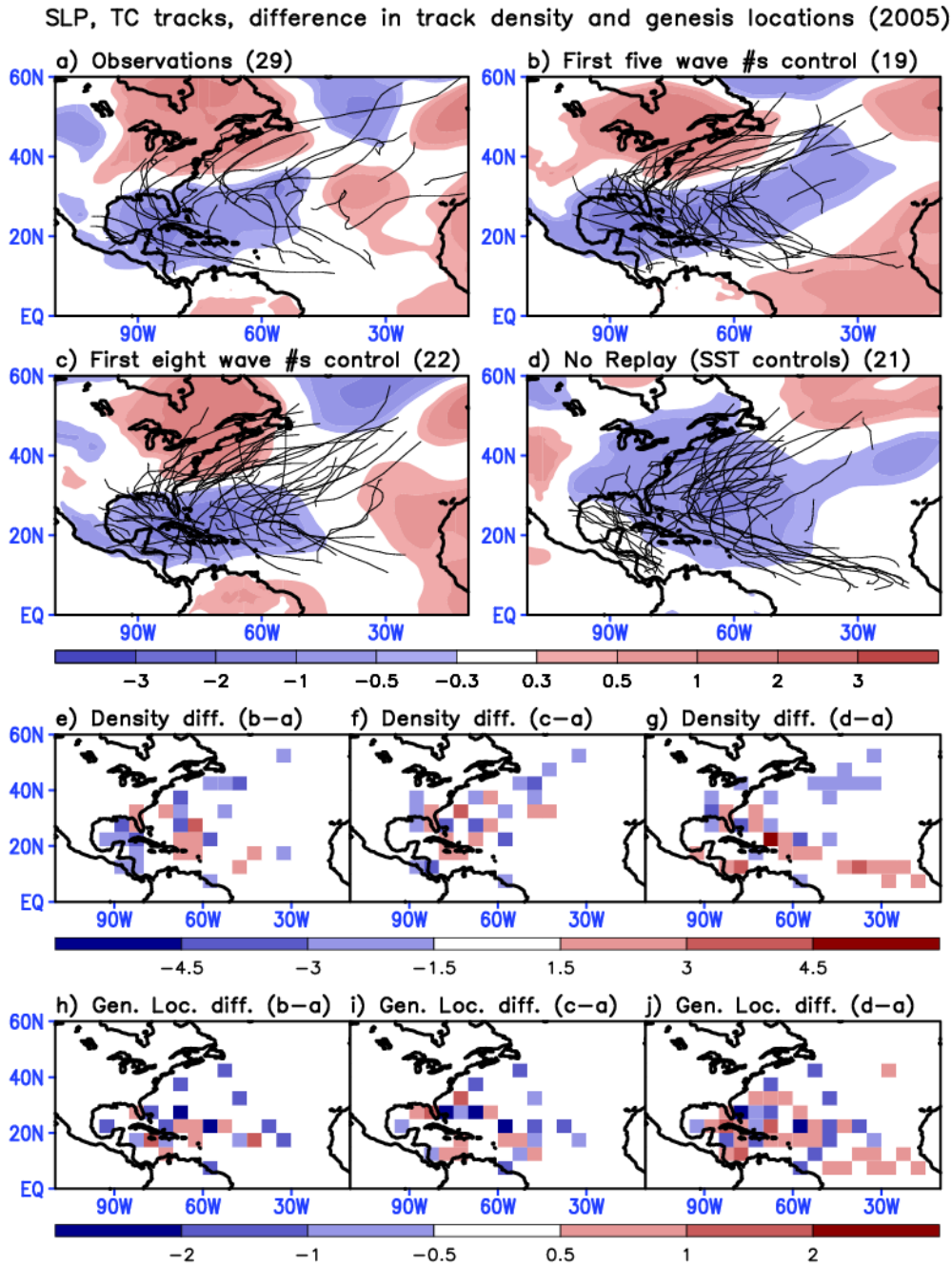
Figure 2. TC tracks for 2005 for a) observations, b) R5W, c) R8W and d) NR. All TC tracks produced by three member runs are plotted for R5W, R8W, and NR. Shading represents the three-member-averaged SLP anomaly for 2005. Number in parentheses above each panel is the average number of detected TCs across the three members. Panels of e, f, and g are distribution of differences in TC track density between model and observation (a). Bottom panels (h, i, and j) are distribution of differences in TC genesis locations between model and observation (a).

Figure 3. Same as Figure 2 but for 2006.

Figure 4. Same as Figure 2 but for 2010.

Figure 5. Same as Figure 2 but for 2013.

Figure 6. The first three rotated empirical orthogonal functions (REOFs) of the observed monthly SST for summer (June to September). The left panel represents the distribution of non-normalized eigenvectors whereas the right panel represents the corresponding PC time series (black solid line). Time series in blue solid lines denote, from the top to bottom panel, the Niño3.4 SST (top), NAO index (middle) and AMM index multiplied by 0.5 (bottom).

Figure 7. Anomaly distributions of the SLP (top row), relative humidity at 700hPa (second row), vertical wind shear (u(150hPa) minus u(850hPa)) (third row) and height at 250hPa (bottom row) regressed onto ENSO. Hatching in the third row panels represents climatologically the easterly wind shear region from observations. Each panel from the left represents the result for observation (first), R8W (second), R5W (third), and NR (fourth).

Figure 8. Same as Figure 7 but for the NAO.

Figure 9. Same as Figure 7 but for the AMM.

Figure 10. Distribution of SLP anomaly resulting from the combined effect of the ENSO, NAO and AMM. From the top to bottom panel, each panel represents the result for 2005, 2006, 2010 and 2013. Each panel from the left represents the result for observation (left), R8W (middle), and NR (right).

Figure 11. Same as Figure 10 but for vertical wind shear (u(150hPa) minus u(850hPa)) (shaded) and relative humidity at 700hPa (contoured). Sold contour lines represent the positive relative humidity anomaly whereas the dashed contours represent the negative anomaly.

Figure 12. Distribution of SLP and SST anomalies from R8W for the combined impact of ENSO and NAO for two active TC years of 2005 (top panel) and 2010 (bottom panel). The different SST and SLP pattern likely causes different TC tracks and genesis locations for two active TC years of 2005 and 2010.

Figure 13. Left panel: Spatial anomaly distribution of z250 associated with ENSO (top), NAO (middle), and AMM (bottom) mode, respectively, captured from 20-member NR run data. Light green contours represent results from each member, and their average is contoured black. Variance in percentage averaged over 20 members is shown above each panel. Right panel: Temporal variation (PC time series) of each mode shown on the left panel. Temporal variations identified from each member are plotted by red-dashed lines, and black solid line with closed-circle represents their average. Time series in blue solid lines denote the Niño3.4 SST (top), NAO index (middle) and AMM index multiplied by 0.5 (bottom).

Figure 14. Signal-to-noise (S/N) ratio distributions of monthly variation of three leading modes (spatial distributions and their temporal variation) predicted by 20-member NR runs. The leading modes represented by SLP are shown on the left panel whereas the left panel the z250. S/N ratio lies in the range of 0 to 1. S/N ratio increases with decrease in intra-ensemble variance (i.e., residual variance).

"Replay" at GMAO: Flow Diagram

Figure 1. A schematic view of replaying the GEOS-5 model to an existing atmospheric analysis dataset. The process is generalized here to apply a filter to the full increments to allow constraining a subset of the flow.

Figure 2. TC tracks for 2005 for a) observations, b) R5W, c) R8W and d) NR. All TC tracks produced by three member runs are plotted for R5W, R8W, and NR. Shading represents the three-member-averaged SLP anomaly for 2005. Number in parentheses above each panel is the average number of detected TCs across the three members. Panels of e, f, and g are distribution of differences in TC track density between model and observation (a). Bottom panels (h, i, and j) are distribution of differences in TC genesis locations between model and observation (a).

Figure 3. Same as Figure 2 but for 2006.

40

979
980
981
982
983
984
985
986
987
988
989
990
991
992
993
994
995
996
997
998
999
1000
1001
1002
1003
1004
1005
1006
1007
1008
1009
1010
1011
1012
1013
1014
1015
1016
1017
1018
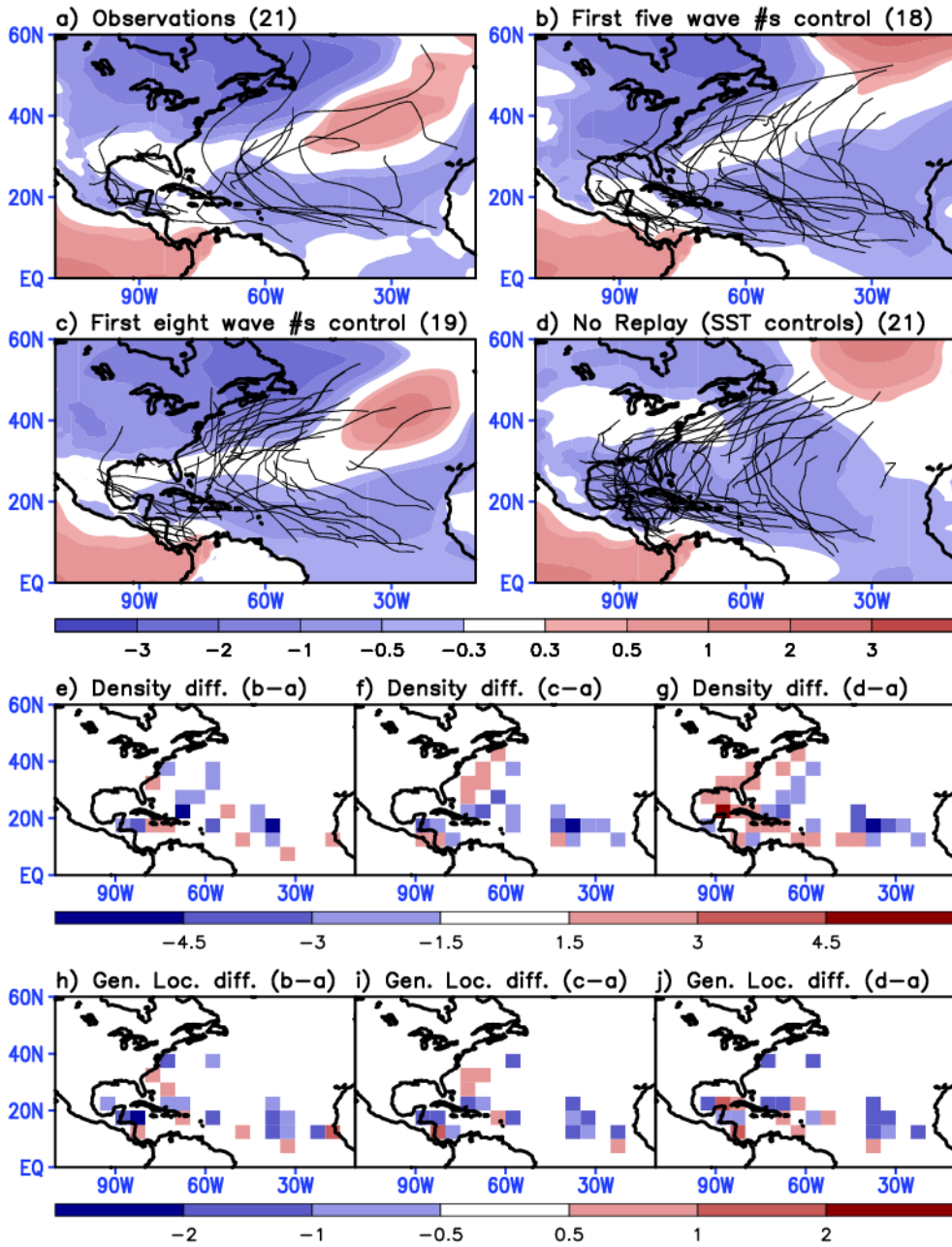
Figure 4. Same as Figure 2 but for 2010.

1019
1020
1021
1022
1023
1024
1025
1026
1027
1028
1029
1030
1031
1032
1033
1034
1035
1036
1037
1038
1039
1040
1041
1042
1043
1044
1045
1046
1047
1048
1049
1050
1051
1052
1053
1054
1055
1056

Figure 5. Same as Figure 2 but for 2013.

Figure 6. The first three rotated empirical orthogonal functions (REOFs) of the observed monthly SST for summer (June to September). The left panel represents the distribution of non-normalized eigenvectors whereas the right panel represents the corresponding PC time series (black solid line). Time series in blue solid lines denote, from the top to bottom panel, the Niño3.4 SST (top), NAO index (middle) and AMM index multiplied by 0.5 (bottom).

Figure 7. Anomaly distributions of the SLP (top row), relative humidity at 700hPa (second row), vertical wind shear (u(150hPa) minus u(850hPa)) (third row) and height at 250hPa (bottom row) regressed onto ENSO. Hatching in the third row panels represents climatologically the easterly wind shear region from observations. Each panel from the left represents the result for observation (first), R8W (second), R5W (third), and NR (fourth).

Figure 8. Same as Figure 7 but for the NAO.

1188
1189
1190
1191
1192
1193
1194
1195
1196
1197
1198
1199
1200
1201
1202
1203
1204
1205
1206
1207
1208
1209
1210
1211
1212
1213
1214
1215
1216
1217
1218
1219
1220
1221
1222
1223
1224
1225
1226
1227
1228

Figure 9. Same as Figure 7 but for the AMM.

46

Figure 10. Distribution of SLP anomaly resulting from the combined effect of the ENSO, NAO and AMM. From the top to bottom panel, each panel represents the result for 2005, 2006, 2010 and 2013. Each panel from the left represents the result for observation (left), R8W (middle), and NR (right).

Figure 11. Same as Figure 10 but for vertical wind shear (u(150hPa) minus u(850hPa)) (shaded) and relative humidity at 700hPa (contoured). Sold contour lines represent the positive relative humidity anomaly whereas the dashed contours represent the negative anomaly.

Figure 12. Distribution of SLP and SST anomalies from R8W for the combined impact of ENSO and NAO for two active TC years of 2005 (top panel) and 2010 (bottom panel). The different SST and SLP pattern likely causes different TC tracks and genesis locations for two active TC years of 2005 and 2010.
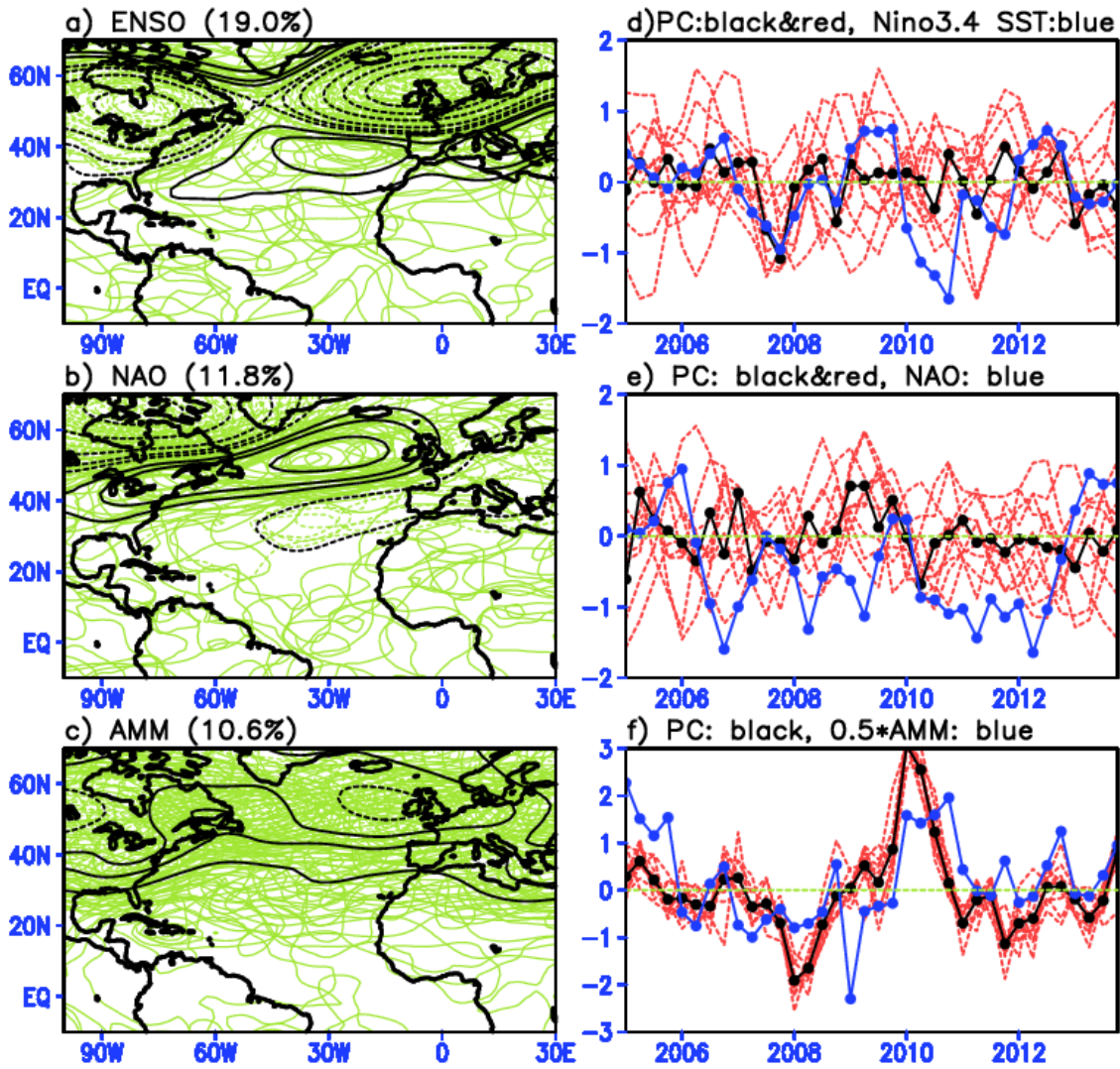
Figure 13. Left panel: Spatial anomaly distribution of z250 associated with ENSO (top), NAO (middle), and AMM (bottom) mode, respectively, captured from 20-member NR run data. Light green contours represent results from each member, and their average is contoured black. Variance in percentage averaged over 20 members is shown above each panel. Right panel: Temporal variation (PC time series) of each mode shown on the left panel. Temporal variations identified from each member are plotted by red-dashed lines, and black solid line with closed-circle represents their average. Time series in blue solid lines denote the Niño3.4 SST (top), NAO index (middle) and AMM index multiplied by 0.5 (bottom).

1394
1395
1396
1397
1398
1399
1400
1401
1402
1403
1404
1405
1406
1407
1408
1409
1410
1411
1412
1413
1414
1415
1416
1417
1418
1419
1420
1421
1422
1423
1424
1425
1426
1427
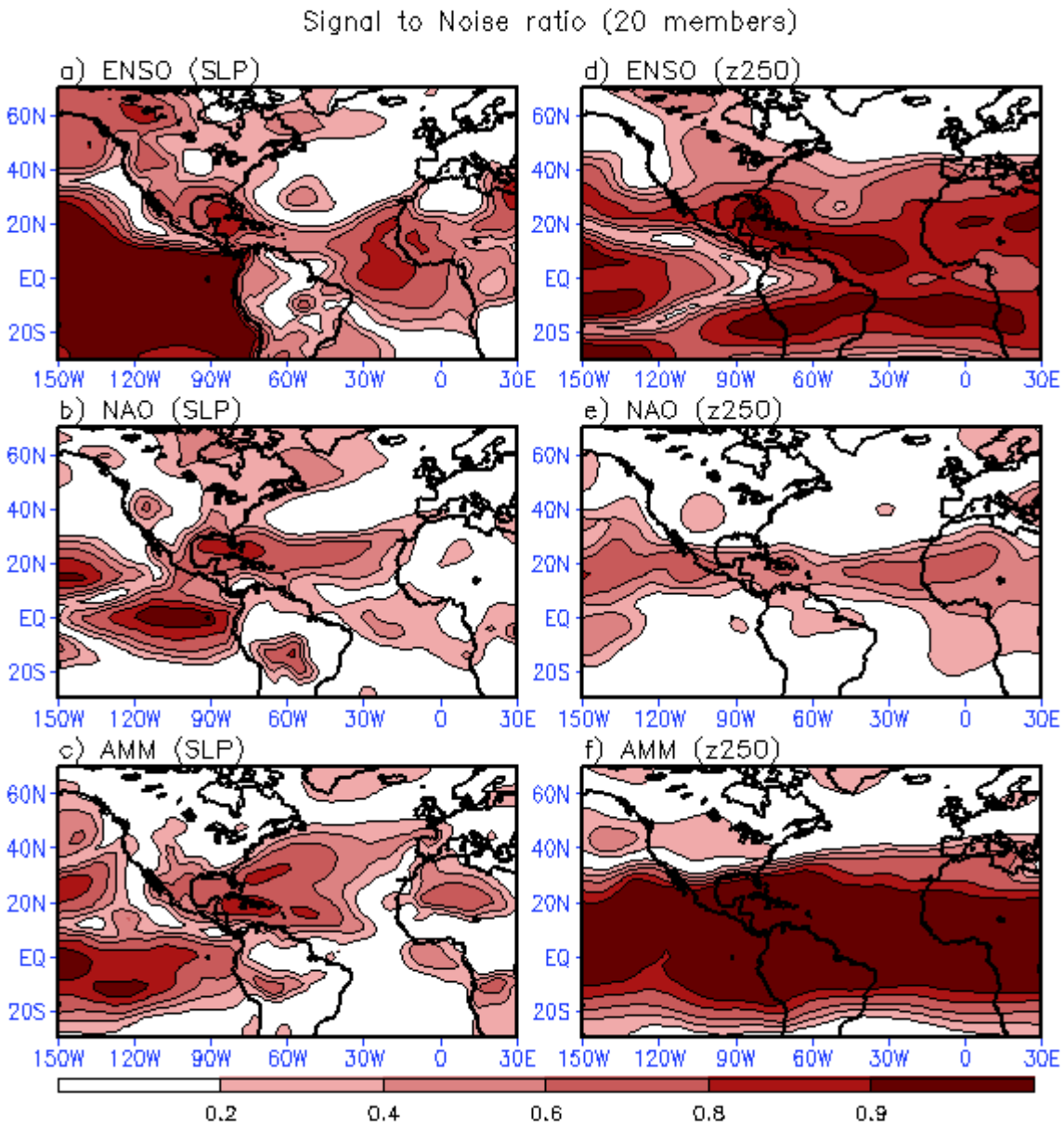1428
1429
1430
1431
1432
1433
1434
1435
1436
1437
1438

1439

Figure 14. Signal-to-noise (S/N) ratio distributions of monthly variation of three leading modes (spatial distributions and their temporal variation) predicted by 20-member NR runs. The leading modes represented by SLP are shown on the left panel whereas the left panel the z250. S/N ratio lies in the range of 0 to 1. S/N ratio increases with decrease in intra-ensemble variance (i.e., residual variance).